ACS APPLIED MATERIALS & INTERFACES

www.acsami.org

Research Article

Assessment of the Behaviors of an In Vitro Brain Model On-Chip under Shockwave Impacts

Md Fazlay Rubby,[¶] Catherine Fonder,[¶] Sajid Uchayash, Xiaogan Liang, Donald S. Sakaguchi,* and Long Que*

Cite This: https://doi.org/10.1021/acsami.4c08026

Read Online

ACCESS | Metrics & More | Article Recommendations | Supporting Information

ABSTRACT: Herein we report the assessment of the effects of shockwave (SW) impacts on adult rat hippocampal progenitor cell (AHPC) neurospheres (NSs), which are used as in vitro brain models, for enhancing our understanding of the mechanisms of traumatic brain injury (TBI). The assessment has been achieved by using culture dishes and a new microchip. The microchip allows the chemicals released from the brain models cultured inside the cell culture chamber under SW impacts to diffuse to the nanosensors in adjacent sensor chambers through built-in diffusion barriers, which are used to prevent the cells from entering the sensor chambers, thereby mitigating the biofouling issues of the sensor surface. Experiments showed the negative impact of the SW on the viability, proliferation, and differentiation of the cells within the NSs. A qPCR gene expression analysis was performed and appeared to confirm some of the immunocytochemistry (ICC) results. Finally, we demonstrated that the microchip can be used to monitor lactate dehydrogenase (LDH) released from the AHPC-NSs subjected to SW impacts. As expected, LDH levels changed when AHPC-NSs were injured by SW impacts, verifying this chip can be used for assessing the degrees of injuries to AHPC-NSs by monitoring LDH levels. Taken together, these results suggest the feasibility of using the chip to better understand the interactions between SW impacts and in vitro brain models, paving the way for potentially establishing in vitro TBI models on a chip.

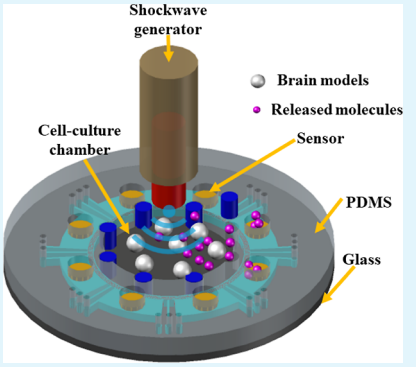

KEYWORDS: *neurospheres, in vitro brain model, shockwave, traumatic brain injury, neural damage monitoring, lactate dehydrogenase*

1. INTRODUCTION

Approximately 70 million people globally sustain traumatic brain injury (TBI) each year, which can have tremendous socioeconomic impacts on their families and society.[1−4] However, because of a lack of understanding of the pathobiological mechanisms of TBI,[5] acute and chronic treatment for brain-injured patients has not kept pace.

Depending on the levels of severity, a TBI can be categorized as mild, moderate, or severe TBI.[6] Among them, mild TBI has the highest incidence in the USA,[7] which occurs in athletes, military personnel, and children who have experienced physical abuse.[8] Given its significant health and economic burdens on the victims, it is of great importance to efficiently diagnose and treat TBI. Toward this goal, animal models such as rodent models have been widely used to study the biomechanical mechanisms and molecular cascades resulting from TBI.[9] These models include cortical impact injury,[10] fluid percussion injury,[11] weight-drop impact acceleration injury,[12] and blast injury.[13,14] Currently, rodent models are used in most TBI research because of their accessibility and low cost, even though TBI models developed for higher order species, such as miniature swine and primate models, are available.[15−17] However, the underlying mechanism for TBI remains poorly understood, due to ethical and/or financial issues for using animal and human models.

While animal and human models are critical for understanding the TBI mechanism and are widely used for improving preclinical testing,[18−20] in vitro models can provide many advantages over animal or human models. Specifically, in comparison with animal models, in vitro models of TBI can provide a cost-effective platform that can develop pathology more quickly and requires no ethical approval, allowing investigators to conduct repeatable, well-controlled, environmentally isolated experiments at a large scale in a short time. In addition, it is easier to achieve genetic or pharmacological manipulations and obtain reliable and time-lapse imaging for analysis.

Some in vitro TBI models have been reported at the cell or tissue level in recent decades.[21,22] Immortalized cell lines have often been used for in vitro two-dimensional (2D) models. Furthermore, dissociated primary cultures do not reliably recapitulate cell−cell interactions in higher dimensions and the dynamic extracellular matrix environment.[5] To address these

Received: May 15, 2024
Revised: June 5, 2024
Accepted: June 8, 2024

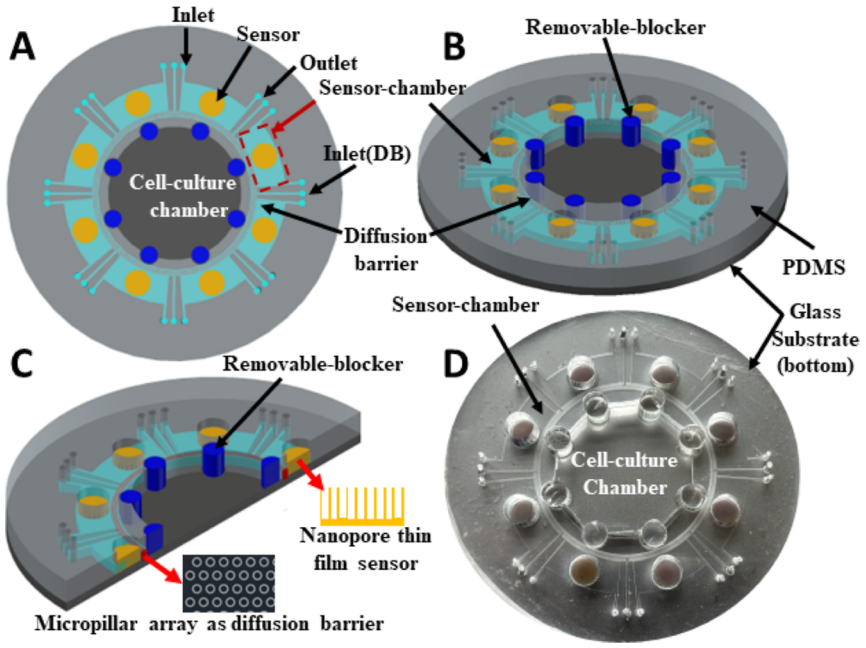

Figure 1. Schematic illustration and the fabricated chip for assessing shockwave impact on NSs. (A,B) Topside and angled view of the chip consisting of one cell-culture chamber (diameter 35 mm) separated by a diffusion barrier (4 row misaligned micropillars, each 150 μm dia.) with eight sensor chambers (15 mm × 6.5 mm each); a nanopore thin-film sensor (diameter 5.5 mm. each) is integrated inside each sensor chamber; eight removeable blockers (diameter 4.5 mm. each) are used to allow culture media to diffuse to eight chambers in sequence; (C) topside view showing the diffusion barrier with micropillar array and cross-sectional view showing the nanopore thin-film sensor; (D) photo of a fabricated chip (~76 mm diameter and thickness 5 mm).

issues, three-dimensional (3D) models have been proposed.[23−25] For instance, in vitro 3D models based on organotypic cultures or acute ex vivo preparations using small animals' brain tissues were developed.[26−29] Recently a 3D printed device has been developed for studying the mechanical mini-impacts on 3D cultured induced pluripotent stem cell (iPSC) derived neural progenitor cells (NPCs),[30] showing great potential to develop an in vitro TBI model by allowing the studies of repeated weight-drop impact injury to the 3D cultured NPC neurospheres (NSs). However, there are still some limitations to current in vitro models. To the best of our knowledge, very few reported technical platforms have been developed that allow (i) real-time monitoring of chemicals/biomarkers released from the healthy models and the models with different levels of injuries;[31] (ii) real-time monitoring of the effects of the healthy models and the injured models with drug treatment; and (iii) large-scale studies of the TBI models with various/different and quantitative mechanical stimuli/damage, especially under shock wave (SW) on a chip simultaneously. These capabilities would tremendously facilitate studies of the central nervous system (CNS)/brain function following TBI under different conditions, enabling high-throughput drug discovery for TBI. As such, a new simple-to-operate technology platform is critically needed. In other words, a new technology platform, which can rapidly generate tens or hundreds of in vitro models with various/different and quantitative injury conditions on a chip, would provide an ideal platform for building in vitro TBI models and achieving high-throughput drug screening.

Herein, we report the development of an integrated chip for studying the effects of SW on in vitro brain models. The brain models are composed of adult rat hippocampal progenitor cells (AHPC) neurospheres (AHPC-NSs).[32,33] As multipotent neural stem cells, AHPCs can differentiate into the three primary cell types of the CNS: neurons, oligodendrocytes, and astrocytes.[34] During culturing without extracellular matrix proteins, AHPCs can self-assemble and maintain their proliferative capacity to generate 3D cellular aggregates and NSs, resulting in greater cell−cell communication and interactions compared to traditional 2D cell culture methods. In this work, we examined the effects of the SW on the viability, proliferation, and differentiation of APHC-NSs and monitored the secretion of chemicals from APHC-NSs subjected to SW impacts. Specifically, we monitored lactate dehydrogenase (LDH) released by AHPC-NSs subjected to SW impacts. LDH is a protein found in most tissues of the human body, including brain tissue.[35] Following tissue damage, they release LDH into the bloodstream or other body fluids.[30,36−39] In other words, if LDH in blood or body fluid levels rises, certain tissues may have been damaged by disease or injury. This chip for in vitro TBI models can be easily extended for monitoring other chemicals released by the brain models subjected to different degrees of SW impacts. Hence it provides an efficient technical platform to study TBI mechanisms, which is readily replicable and can be potentially used for high-throughput drug screening.

As shown in Figure 1, the AHPC-NSs (i.e., the mini-brain models) are cultured in a cell culture chamber separated by a diffusion barrier from eight chambers containing nanosensors fabricated from nanopore thin film.[40] The diffusion barrier consists of arrayed misaligned micropillars to prevent the AHPC-NSs in the cell culture chamber from migrating to the sensor chambers to mitigate the biofouling of the sensor surface. Meanwhile, the secreted chemicals from AHPC-NSs can diffuse to the sensors and be monitored. The eight chambers are physically separated from each other, allowing the sensor in each chamber to monitor the chemicals released

https://doi.org/10.1021/acsami.4c08026
ACS Appl. Mater. Interfaces XXXX, XXX, XXX−XXX

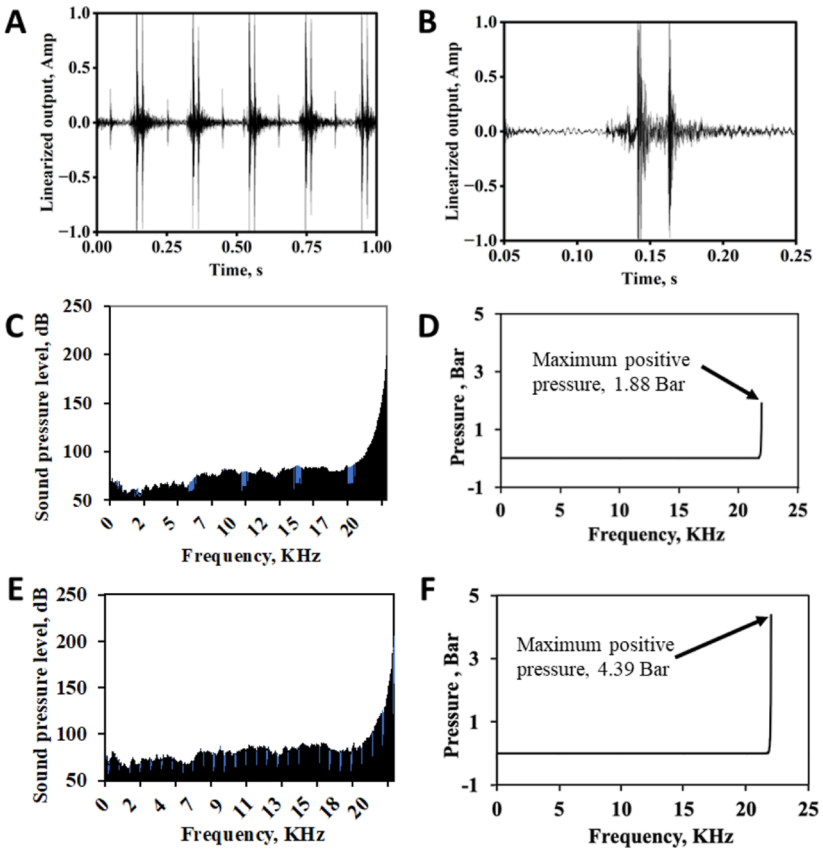

Figure 2. Shockwave characterization. (A) Shockwave output (5 Hz) from a SW generator probe (Kalecope, Inc.) recorded by a hydrophone; (B) shockwave output (1 pulse); (C,D) FFT of 1 pulse of shockwave (2 bar) and its pressure conversion; and (E,F) FFT of 1 pulse (4.5 bar) and its pressure conversion.

from the brain models subjected to SW impacts at different time points.

2. MATERIALS AND METHODS

2.1. Chemicals and Materials. *2.1.1. For Chip Fabrication.* Positive photoresist AZ 40XT and AZ 326 MIF developer were purchased from MicroChemicals (Germany). Polydimethylsiloxane (PDMS) and curing agents (SYLGARD 184 Silicon Elastomer Kit, 2-part) were purchased from Dow Corning (Midland, MI, USA). Aluminum targets of high purity (99.99%) were purchased from Kurt J. Lesker, Inc. Deionized (DI) water was made by tap water through a DI water purification system (Millipore, USA).

2.1.2. For Cell Culture and Cell Viability Examination. Adult rat hippocampal progenitor cells (AHPCs) were generously gifted by Dr. F.H. Gage, Salk Institute, La Jolla, CA. Poly-L-ornithine solution (catalog #50-165-6954) was purchased from Sigma-Aldrich (St. Louis, MO). Laminin was purchased from Cultrex by Trevigen (catalog #340001002) (Gaithersburg, MD). Dulbecco's modified Eagle's medium/Ham's F-12 (DMEM/F-12, 1:1) (catalog #NC9868086), GlutaMAX (catalog #35050061), N2 supplement (catalog #17502048), penicillin/streptomycin (catalog #15140122), basic fibroblastic growth factor (bFGF) (catalog #PRG5071), uncoated tissue-culture polystyrene (TCPS) culture-ware, and propidium iodide (PI) (catalog #P4864) were purchased from Thermo Fisher Scientific (Waltham, MA).

2.1.3. For Surface Functionalization of Nanopore Thin-Film Sensors and Detection of LDH. 11-Mercaptoundecanoic acid ($HSC_{10}COOH$, 99%) (catalog #450561), 8-mercapto-1-octanol (HSC_8OH, 98%) (catalog #706922), *N*-(3-(dimethylamino)propyl)-*N*′-ethylcarbodiimide hydrochloride (EDC) (catalog #39391), *N*-hydroxysuccinimide (NHS) (catalog #130672), and ethanolamine (EA) (catalog #15014) were purchased from Sigma-Aldrich, Co. (St. Louis, MO, USA). Rat LDH (lactate dehydrogenase) ELISA Kit was purchased from MyBioSource, Inc. (catalog #MBS8804669).

2.2. Chip Description, Modeling, and Fabrication. *2.2.1. Description and Operation of the Chip.* The chip is schematically shown in Figure 1A–C. It consists of a cell-culture chamber, around which eight sensors are located inside eight sensor chambers. The sensor chambers are isolated from each other and are also separated from the cell-culture chamber by a removable blocker and a diffusion barrier (DB). Each sensor chamber has a pair of inlet and outlet, allowing the chemicals to flow to each chamber for surface functionalization of the sensor surface. There is a third channel with an Inlet(DB) between the sensor chamber inlet and outlet to access the DB region, which can be used to inject curable polymer gel into the barrier region to modulate the diffusivity of the barrier region for future experiments. Each removable blocker can be removed to allow the sensors to detect the chemicals released from in vitro brain models (AHPC-NSs) as they diffuse through the diffusion barrier between the cell chamber and sensor chambers to each sensor in sequence at different time points. A close-up view of the diffusion barrier and the nanopore thin-film sensor is illustrated in Figure 1C. In this design, the diffusion barrier consists of 4–5 rows of micropillars. The adjacent misaligned rows of the micropillars reduce the effective gaps among them. As a result, the fluidic resistance increases, and the passage of AHPC-NSs through the diffusion barrier to the sensor chambers can be significantly minimized;[41] thus the biofouling issues associated with the cells and cellular debris of the sensors can be tremendously mitigated. The gaps among micropillars in the same row or between each row are designed to be 20 μm. A cross-sectional view of the chip and a close-up of the nanosensor are shown in Figure 1C. A photo of a fabricated chip is shown in Figure 1D.

2.2.2. Fabrication of the Chip. (1) Fabrication of the nanopore thin-film sensors: the sensors were fabricated on a glass substrate.

https://doi.org/10.1021/acsami.4c08026
ACS Appl. Mater. Interfaces XXXX, XXX, XXX−XXX

Table 1. Timeline and Reagents for Analyzing SW-Treated AHPC-NSs

	cell viability analysis		differentiation & proliferation analysis	qPCR gene expression analysis
timeline for analysis	3 DIV	7 DIV	7 DIV	7 DIV
fluorescence/antibody marker	PI Stain	PI Stain	TuJ1 × Ki67, RIP × Ki67, MAP2ab × GFAP	TuJ1, NeuN, RIP, GFAP, BCL2, BAX, p53

Briefly (Figure S1A in Supporting Information), a thin film of 3−4 μm of high-purity Al was deposited on the glass substrate using 1−2 nm Ti as an adhesion layer. One-step anodization was performed to convert Al into an anodic aluminum oxide (AAO) nanopore film.[42] A layer of ∼1 μm Al was then deposited on the AAO nanopore film, which was used as a protective layer for AAO during the etching step to fabricate AAO patterns. AAO patterning was carried out using the following steps. First, a photoresist layer was deposited on top of the Al layer. Then using lithography Al layer was etched except for the sensor area. After that, the AAO layer was etched except for the sensor area. Finally, the Al layer was etched from the sensor area and only AAO remained on the sensor area. The AAO patterns were coated with a layer of ∼5 nm Au using ∼1 nm Ti as an adhesion layer using a lift-off process (Figure S1B in Supporting Information). (2) A soft lithography process was used to fabricate the PDMS microfluidic layer. Briefly, a mold was first fabricated from resist AZ40XT. PDMS solution (base and curing agent ratio, 9:1) was then poured on the mold followed by 1 h degassing and overnight curing at 45 °C. Afterward, the PDMS microfluidic layer was peeled off the mold, followed by the formation of the chambers, inlets/outlets, and removable blockers by punching through the PDMS layer using biopsy punchers with different diameters. (3) The fabrication of the chip (Figure S1C in Supporting Information) was completed by bonding the PDMS microfluidic layer to the glass substrate with nanopore thin-film sensors after oxygen plasma treatment.

2.2.3. Shockwave Characterization. A SW generator probe (Kalecope, Inc.) is used to generate SW in our experiments. In this probe, compressed air accelerates a projectile up to 80 to 90 kph within a guiding tube that strikes a metal applicator. The kinetic energy is converted into a radial shock wave. The projectile generates a stress wave in the applicator that can transmit pressure waves into a liquid to a depth of 4 to 5 cm. The shockwave generated by the probe was recorded by a piezoelectric hydrophone (H-instruments, Inc.).[43,44] The average rise time of the SW was recorded as 50−70 μs. The peak pressure was recorded in the range of 1.89 to 4.39 bar. The linearized signal output (5 Hz) is illustrated in Figure 2A. The signal has five pulses in 1 s. The recorded SW was oscillating in nature, which loses its energy with time. One pulse (Figure 2B) was extracted for Fast Fourier transform (FFT) analysis. It shows the sound pressure level of individual frequencies ranging from 0 to 25 kHz. It is illustrated in Figure 2C for a 2 bar SW and Figure 2E for a 4.5 bar SW. The highest sound pressure level was found at a frequency of 22 kHz. Then the sound pressure level was converted to sound pressure (bar) using the following formula, $L_p = 20 \log_{10} (p/p_0)$ dB, where p_0 = reference pressure = 20 μPa, L_p = sound pressure level, and p = sound pressure (bar).[45−48] The converted pressure graphs are given in Figure 2D for the 2 bar SW and Figure 2F for the 4.5 bar SW. The maximum positive pressure measured by the hydrophone from the 2 bar shockwave (mild treatment) was actually ∼1.88 bar and from the 4.5 bar shockwave (moderate treatment) was actually ∼4.39 bar.

2.2.4. Modeling of the SW Impacts on APHC-NSs. Numerical calculations were carried out to simulate the SW impacts on AHPC-NSs using the COMSOL Multiphysics software (COMSOL Inc., Los Angeles, CA, USA). For simplicity, it is assumed that (1) the AHPC-NSs remain at the same locations in the culture media during the SW impacts, (2) Young's modulus of APHC-NSs is 40 kPa,[49] and (3) the SW propagates through the culture media to impact the AHPC-NSs.

2.2.5. AAO Nanopore Thin-Film Sensor Characterization. The nanopore sensor was characterized by measuring the transducing signals of LDH samples of known concentrations. First, the sensor surface was functionalized by the LDH antibody using the protocol developed in our lab.[50,51] Then the optical spectrum was recorded using a spectrometer (OceanOptics, Inc.). After that, the LDH antigens were added to the sensor. Then the second spectrum was recorded after 30 min incubation at room temperature followed by a rigorous phosphate-buffered saline (PBS) rinsing.[50,51] The operational principle of the sensor was reported in our previous publication.[42] The peak shift (nm) of the interference fringes was obtained from those spectra as the transducing signal, which is summarized in Figure S2A,B in the Supporting Information.

2.3. Culturing of AHPC-NSs. The AHPCs were originally isolated from the brains of adult Fischer 344 rats as reported by Palmer and colleagues.[52] AHPC-NSs were formed by culturing AHPCs in uncoated T25 culture flasks using complete AHPC culture maintenance medium (MM) composed of DMEM/F-12, supplemented with 2.5 mM GlutaMAX, 1 × N2 supplement, 1 × penicillin/streptomycin, and 20 ng/mL bFGF. Self-assembly of AHPCs results in the formation of AHPC-NSs that continue to proliferate. To harvest the AHPC-NSs for seeding into the cell chambers of the chip, the NSs cell suspension was collected in a 15 mL conical tube where the NSs pelleted via gravity. After pelleting, the supernatant was removed, and the cells were rinsed three times with 1 mL of fresh MM to remove any debris from the cell suspension. Following the rinses, the NSs were resuspended in 1 mL of fresh MM for seeding. 200 NSs were seeded into either 35 mm culture dishes or the cell-culture chamber of the chip (Figure 1).

2.4. Immunocytochemistry. For all cell staining and immunocytochemical procedures, NSs were collected from one 35 mm dish per experimental condition and transferred to 1.5 mL Eppendorf tubes where the procedures were performed in suspension. Briefly, the NSs were rinsed with 0.1 M PO_4 buffer for 1 min before incubating in 4% paraformaldehyde (catalog #AC416780250) (PFA, Thermo Fisher Scientific) in 0.1 M PO_4 buffer for 20 min. The fixation was followed by three, 7 min PBS rinses for complete removal of the fixative. The cells were then incubated in blocking solution composed of 0.2% Triton X-100 (catalog #BP151−100) (Thermo Fisher Scientific), 5% normal donkey serum (catalog #NC9624464) (NDS) (Jackson ImmunoResearch), and 0.4% bovine serum albumin (BSA) (Sigma-Aldrich) in PBS at room temperature for 90 min. Primary antibodies Rabbit α Ki-67 (1:200, IgG; Abcam), Mouse α TuJ1 (catalog #MAB1195) (1:200, IgG; R&D Systems), Mouse α MAP2ab (catalog #BDB556320) (1:200, IgG; Sigma-Aldrich), Mouse α RIP (1:200, IgG; DSHB, Iowa City, IA), and Mouse α GFAP-Cy3 conjugated (catalog #C9205) (1:200, IgG; Sigma-Aldrich) were diluted in the blocking solution. The NSs were double-labeled with the following combination of primary antibodies: TuJ1 + Ki67, RIP + Ki67, and MAP2ab + GFAP (Table 1). The cells were incubated in the primary antibody solution overnight at 4 °C, except for GFAP which was not incubated until the following day following secondary antibody incubation for the MAP2ab-labeled samples. After the overnight primary antibody incubation, the samples were rinsed with PBS four times for 8 min each. To prepare the secondary antibody solution, Donkey α Rabbit Cy3 (catalog #711165152) (1:200, IgG; Jackson Immunoresearch) and Donkey α Mouse AF488 (catalog #NC0193319) (1:200, IgG; Jackson ImmunoResearch) were diluted with the blocking solution containing 4′,6-diamidino-2-phenylindole (catalog #D3571) (DAPI; diluted 1:1000; Invitrogen). The cells were incubated with the secondary antibody solution at room temperature in the dark for 90 min after which the samples were rinsed with PBS four times for 8 min each The MAP2ab-labeled samples were then incubated with the GFAP-Cy3 conjugated primary antibody for 60 min and then underwent an additional set of four, 8 min PBS rinses.

2.5. PI Staining and Cell Viability Assessment. The cell viability was evaluated using PI to stain dead cells within the NSs. One 35 mm dish sample was used from each experimental condition.

https://doi.org/10.1021/acsami.4c08026
ACS Appl. Mater. Interfaces XXXX, XXX, XXX−XXX

Table 2. Primer Sequences Used for qRT-PCR

genes	forward primer sequence (5′ → 3′)	reverse primer sequence (5′ → 3′)
TuJ1	CAGATAGGGGCCAAGTTCTGG	TCCGAGTCCCCCACATAGTT
NeuN	TGGCTGGAAGCTAAACCCTG	GGGGAAACTGGTCACTGCAT
GFAP	CGAAGAAAACCGCATCACCA	ATTTGGTGTCCAGGCTGGTT
RIP	TATGCCCAACAGGATGTGGT	CAGGTCACTTGGCCACAACT
BAX	ACGTCTGCGGGGAGTCA	CTCGATCCTGGATGAAACCCT
BCL2	TCATGTGTGTGGAGAGCGTC	AGTTCCACAAAGGCATCCCAG
p53	CCCCTGAAGACTGGATAACTGT	ATTAGGTGACCCTGTCGCTG
GAPDH	AGACAGCCGCATCTTCTTGT	CCGATACGGCCAAATCCGTT

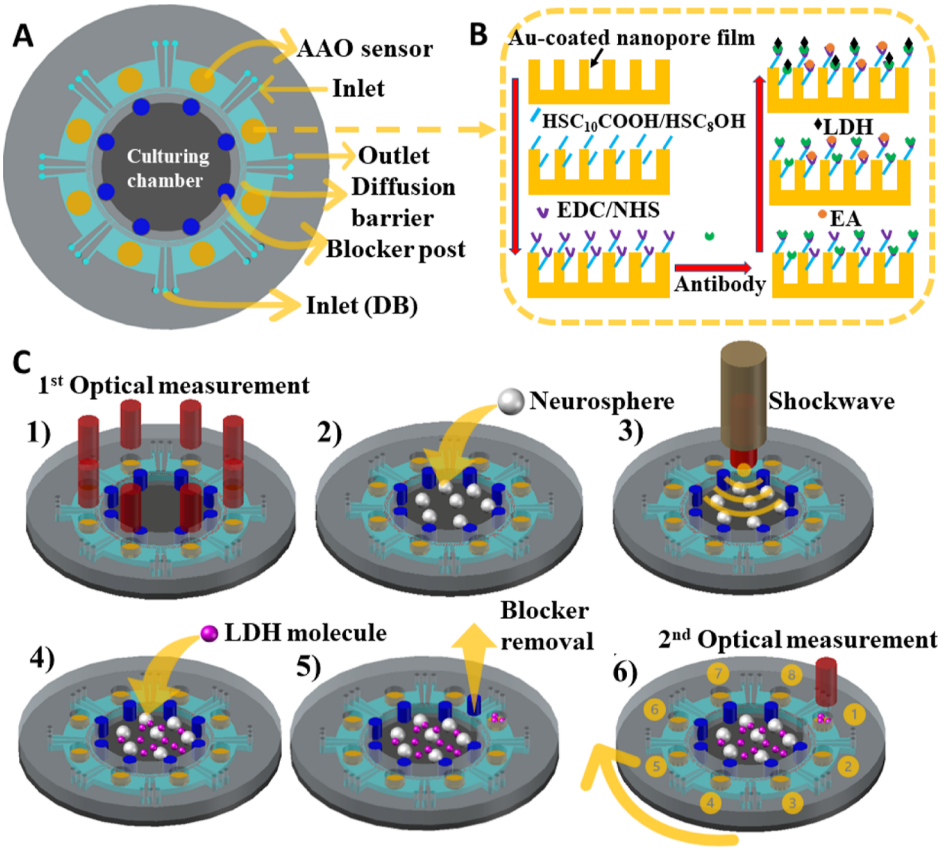

Figure 3. Surface functionalization of the sensor and experiment procedure. (A) Schematic illustration showing the device highlighting the sensors, blocker post, inlet and outlet (sensing chamber), and diffusion barrier; (B) schematic illustration showing the major steps and chemicals through the inlet and outlet of each sensor chamber for realizing sensor surface functionalization; (C) schematic illustration showing (1) experimental sequence of optical measurements, (2) NSs seeding in the culturing chamber, (3) shockwave treatment, (4) LDH molecules release, (5) blocker removal, and (6) final optical measurement of one sensor on chip. The optical measurements are repeated sequentially for the rest of the sensors.

The PI was diluted to 1.5 μM in a cell culture medium. The NSs were incubated in the PI solution for 20 min at 37 °C in 5% CO_2 in 1.5 mL Eppendorf tubes. As a reagent control, a 0.6 mL Eppendorf tube containing a small sample of NSs was incubated with 70% ethanol for 5 min to intentionally kill all cells before adding the PI solution. After PI incubation, the NSs were rinsed with 0.1 M PO_4 buffer for 1 min and then fixed with 4% PFA for 20 min. After, the samples were rinsed with PBS three times for 7 min each. The NSs were then incubated with DAPI (1:1000) diluted in a blocking solution for 60 min at room temperature in the dark after which time, the samples underwent four 8 min rinses with PBS.

2.6. Experimental Procedure to Apply SW on AHPC-NSs and Analysis. AHPC-NSs were cultured in uncoated 35 mm culture dishes for a total of 9 days in vitro (DIV). Briefly, NSs were plated into the dishes at 0 DIV, and cells were maintained in complete AHPC culture medium for the first 48 h. After 48 h, the culture medium was switched to AHPC differentiation medium (MM without bFGF). At the same time, a subset of the AHPCs underwent one application of SW treatment. The SW parameters were as follows: 100 pulses at 5 Hz frequency at a strength of either 2 bar (mild strength) or 4.5 bar (moderate strength) using a SW generation probe (Kalecope, Inc.). The disinfected probe was positioned perpendicularly to the sample surface for the treatment. A parallel set of dishes acted as nonstimulated control cultures. The control dishes were exposed to the SW applicator for the same duration of time as the treated samples, but they were not exposed to the SW pulses. After the single SW treatment, the NSs were maintained for up to an additional 7 DIV in differentiation medium. The NSs underwent cell viability analysis at multiple time points post-treatment to evaluate the effect of SW treatment on cell viability over time. At the end of the 7 DIV period, the remaining dishes were then fixed and immunostained with various neural markers to determine the effects of the SW treatment on differentiation and proliferation within the NSs. Lastly, a qPCR gene expression analysis was conducted to determine differences in the expression of genes related to cell health and differentiation comparing between the SW-treated samples and the

https://doi.org/10.1021/acsami.4c08026
ACS Appl. Mater. Interfaces XXXX, XXX, XXX−XXX

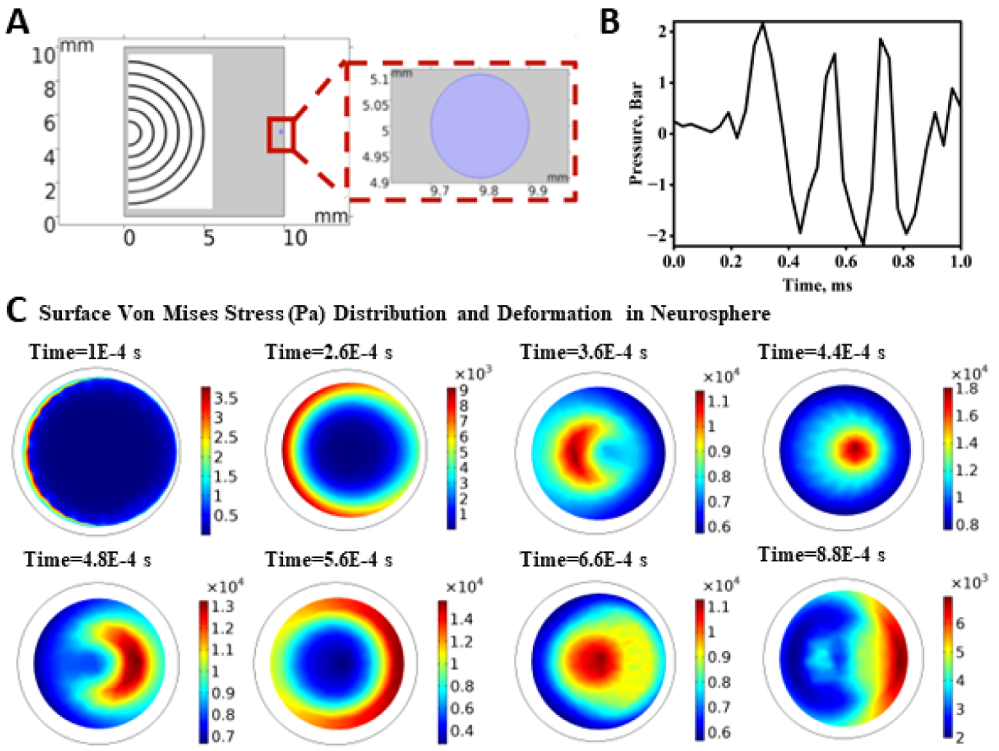

Figure 4. Calculation of SW impacts on a NS. (A) Schematic showing the setup of the model: the propagation of the radial SW toward a NS immersed in culture media at the bottom of a culture chamber; (B) calculated incident pressure profile of the SW immediately impacted on a NS; (C) calculated 2-D pressure profiles across the NS at different time points during 1 ms SW impact. The white circle is the original size of the NS without any SW impact.

nontreated controls. Table 1 lists the timeline for the analyses of post-treatment and the antibodies used or genes tested in the differentiation and gene expression analyses.

2.7. Imaging. To monitor the cell growth and AHPC-NS development during the culture period, a Nikon Diaphot inverted-phase contrast microscope (Nikon Corp.) equipped with a Q Imaging Retiga 2000R (Q Imaging) digital camera was used to take daily phase contrast images of AHPC-NSs. To image the PI staining and immunocytochemistry results, 20 μL of Fluoromount was added to the surface of a microscope slide and 10−15 μL of the stained or immunolabeled NSs within the Eppendorf tubes was added to the center of the 20 μL Fluoromount droplet. A coverslip was placed over the droplet to permanently mount the NSs for imaging. Fluorescence images of a single focal plane of the NSs within the mounted samples were taken using a Nikon Microphot FXA (Nikon Corp.) microscope equipped with standard epifluorescence illumination and a Q Imaging Retiga 2000R (Q Imaging) digital camera. For a focal plane to be selected for imaging, the plane needed to exhibit the highest number of cells in focus compared to all other focal planes visible for the sphere. Each image captured contained a single NS. A 20× objective was used to obtain images for quantitative data analysis.

2.8. Gene Expression Analysis. RNA was extracted from one 35 mm dish sample per condition using the RNeasy Plus Mini Kit (Qiagen, Hilden, Germany) as per the manufacturer's instructions. A nanodrop was used to quantify the amount of RNA in each sample and confirm the RNA isolation's purity with the A280/A260 values ranging from 2.0 to 2.2 for all samples. After isolation, RNA was stored at −80 °C until used for analysis.

Primers were designed using the NCBI gene reference database and Primer-BLAST program.[53] Primer sequences can be found in Table 2. qRT-PCR reactions were performed using the Applied Biosystems Power SYBR Green RNA-to-CT 1-Step kit (Thermo Fisher Scientific, Waltham, MA) as per the manufacturer's instructions. 200 nM of each primer and 100 ng of RNA template were used to prepare the RT-PCR reactions.

Gene expression for each condition was determined using the ΔΔCt method, with expression normalized to the housekeeping gene GAPDH. Reactions were carried out using a QuantStudio 3 real-time PCR instrument. Three independent biological replicates were used for data analysis with each biological replicate run in technical duplicates or triplicates and included a negative control.

2.9. Data Acquisition and Statistical Analysis. The images of NSs were analyzed and quantified using ImageJ software (http://imagej.nih.gov/ij). *Ki*-67, TuJ1, MAP2ab, RIP, and GFAP immuno-positive cells were counted using the Cell Counter tool in ImageJ, and the percentage of immunoreactive cells was determined as the number of positively labeled cells over the total number of cells as determined by the number of DAPI-labeled nuclei.

All means are reported with standard error of the mean (mean ± SEM). Graph Pad Prism 9 (Graph Pad Software, Inc. San Diego, CA) was used for statistical analysis and graph-making. Means were compared using ordinary one-way ANOVA. Statistical significance was determined using Tukey's multiple comparison test, with alpha = 0.05.

2.10. Experimental Procedure to Measure LDH. After the completion of surface functionalization of the nanosensors as illustrated in Figure 3A,B,[51] the chips were sterilized using 70% ethanol. Care was taken during this step by not spraying the ethanol onto the sensor surface since it might damage the surface functionalization. Afterward, the chips were soaked with sterilized filtered PBS solution overnight to allow the PDMS layer of the chip to be saturated with liquid/solution. As a result, the loss of cell culturing media from the chip can be mitigated during the incubation period. After that, AHPC-NSs were plated and cultured in uncoated cell culture chambers on six chips with a diameter of 35 mm for 8 DIV. Specifically, NSs were plated into the cell culture chambers at 0 DIV and were maintained in complete AHPC culture medium for the first 48 h. After 48 h, the culture medium was switched to AHPC differentiation medium. AHPC-NSs on four chips underwent one application of SW treatment at 2 DIV. A SW generator probe (Kalecope, Inc.) for applying SW on the AHPC-NSs is illustrated in

https://doi.org/10.1021/acsami.4c08026
ACS Appl. Mater. Interfaces XXXX, XXX, XXX−XXX

Figure 3C. Again, the disinfected probe is positioned perpendicularly to the sample surface. The SW parameters were as follows: 100 pulses at 5 Hz frequency at a strength of 2 bar. After the single SW treatment, the NSs on chips were cultured for up to an additional 6 DIV in differentiation media. Among the four chips, two chips underwent another application of SW treatment at 4 DIV. The SW parameters remained the same as in the first application. The remaining two chips with cultured AHPC-NSs were used as nonstimulated controls. The NSs on these chips were exposed to the SW probe for the same duration of time as the treated NSs but not exposed to the SW pulses.

During the procedure, measurements were taken on each of the sensors arranged around the 35 mm cell culture chamber in sequence. The removable PDMS blockers between the cell culture chamber and the adjacent sensor chamber were removed to allow the culture medium to flow to the sensor one by one each day in sequence. Specifically, at 0 DIV only one blocker was removed, allowing the cultural medium to enter the adjacent sensor chamber so that the LDH could be conjugated with a precoated antibody specific to LDH. Afterward, the AHPC-NSs were incubated for 24 h before triple measurements were taken on the sensor. The key steps of the experimental procedures for the first sensor are highlighted in Figure 3C. A similar procedure was followed for the rest of the sensor chambers and sensors.

The detailed procedure for the measurements from the sensors was illustrated in previous publications.[51] Briefly, an optical fiber probe (Ocean Optics, Inc.) delivered white light perpendicularly to the sensor surface, the reflected light was collected by the same optical fiber probe, leading to a miniature spectrometer (Ocean Optics, Inc.). The measured transducing signal is the peak shift ($\Delta\lambda$) of optical interference fringes (Figure S2A in Supporting Information). After collecting the data, the shifts of the optical signals were averaged, resulting in the transducing signals. It is worth noting that the control experiments may cause some level of spectral shift in the optical signal likely due to nonspecific binding of the molecules. The shift was considered a background shift, which was subtracted from all measured results. All data were presented in mean ± SD. Independent experiments for each of the eight samples were performed at least three times.

3. RESULTS AND DISCUSSION

3.1. Calculation of SW Effects on AHPC-NSs. The simulation of SW impacts on AHPC-NSs was done using the finite element analysis method (COMSOL Multiphysics) by solving the governing equations of SW and the elasticity of the solid structure (i.e., AHPC-NSs). The coupling between SW and structural physics was used to assess the effects of SW on NSs.

The schematic of the model is presented in Figure 4A for one AHPC-NS under SW treatment. The AHPC-NS was modeled as a circle of 100 μm radius, comparable to that in the experiments, at the bottom of the cell culturing dish. The AHPC-NSs were submerged within the culture media. During the SW applications, the SW probe touched the media surface. The top surface of the media was modeled as the source of the incident SW. The distance between the SW probe and the AHPC-NS was approximately 10 mm, similar to that in the experiments. The properties of cultural media and the NSs in the simulation are summarized in Table 3.[49,54−56]

The pressure pulse recorded from the hydrophone was used as an input pulse for the numerical simulation. Only 1 ms of pressure pulse was chosen to reduce the calculation time. It should serve our goal to observe the stresses developed in the NS during the positive/negative pressure pulse. The profile of the stresses in the NS repeats itself in the other phase of the pressure pulse. Initial SW pressure within the culture media is set to zero. The calculated SW pressure profile at the front of the AHPC-NS is shown in Figure 4B during SW treatments. The distribution of von Mises stress across the AHPC-NS and the deformation of the AHPC-NS at different time points are depicted in Figure 4C. During the SW operation period, it was observed that the NS was always under compression. For comparison, the white circle in Figure 4C indicates the original size of the NS. At time t = 0.26 ms, the highest stress (9×10^3 Pa) was observed along the top periphery of the NS. At time t = 0.36 ms, the highest stress (1.1×10^4 Pa) was observed near the center of the NS. The highest stress was observed (1.8×10^4 Pa) at 0.44 ms in the middle (smaller circular zone) of the NS. At time t = 0.56 ms, the highest stress (1.6×10^4 Pa) was observed at the bottom periphery of the NS. At time t = 0.88 ms, the highest stress (7×10^3 Pa) was observed at the bottom side (semicircular zone) of the NS. The SW propagated through the NS from top to bottom, and thus the NS was under different stress profiles at different time points during 1 ms SW treatment. Several AHPC-NSs under SW treatment have been modeled. Some representative results are given in the supplementary document (Figure S3 in Supporting Information). As expected, the stress profiles on AHPC-NSs subjected to the SW impacts are dependent on their locations in the cell culturing dish or the cell-culture chamber on a chip (Figure S4 in the Supporting Information). The validation of our numerical model was also performed (Figure S5 in the Supporting Information).

Table 3. Major Parameters of Culture Media and AHPC-NSs Used in the Simulation

culture media	speed of shockwave (sound)	1510 m/s	54
	density	1011 kg/m^3	54
AHPC-NSs	Young's modulus	40 kPa	49
	Poisson's ratio	0.38	55
	density	1000 kg/m^3	56

3.2. SW Effects on AHPC-NSs: Viability, Proliferation, and Differentiation. *3.2.1. Cell Viability.* After SW treatment, the quality of the NSs in the culture dishes that underwent either mild SW (2 bar) or moderate SW (4.5 bar) treatment appeared to degrade. Overall, the treated NSs tended to have a more ragged appearance with less defined edges. The NSs themselves were more likely to appear less spherical or deformed compared to the nonexposed controls, which retained a spherical shape throughout the culture period (Figure 5A−C). The treated NSs were also found to be more fragile compared to their nonexposed counterparts as the treated NSs were more likely to be dissociated or broken apart during processing. All these characteristics indicate there was a decrease in the health of the cells within these NSs after mild or moderate SW treatment.

To evaluate the viability of the cells within the NSs with or without SW treatment, PI staining was used to mark dead cells within the cultures. When comparing the differences between the exposed conditions after staining, it was difficult to distinguish qualitatively if there was a significant difference between the percent of PI-labeled cells between the mild and moderate treatments at either the 3 or 7 DIV time points; however, both SW-exposed conditions appeared to have much higher amounts of PI staining compared to the control condition (Figure 5D,E). Overall, the moderate treatment condition resulted in the greatest number of PI-labeled cells compared to all other conditions. No clear trend in the localization of the nonviable cells within the NSs was observed

https://doi.org/10.1021/acsami.4c08026
ACS Appl. Mater. Interfaces XXXX, XXX, XXX−XXX

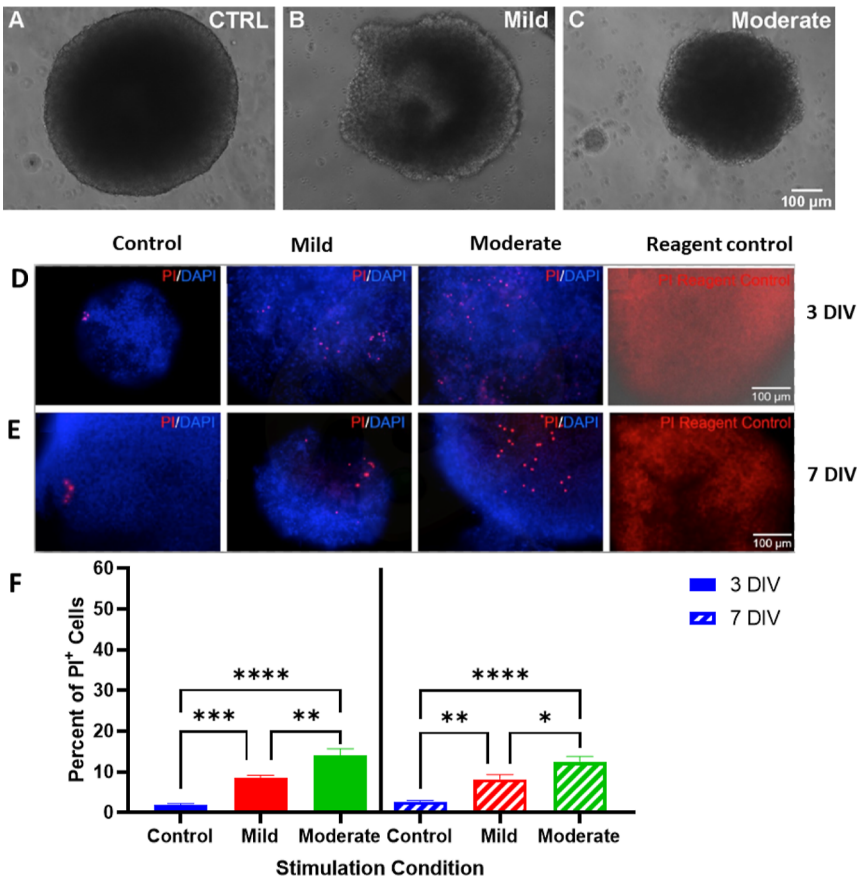

Figure 5. Comparison of NSs 7 days after shockwave treatment & viability of AHPC-NSs at 3 and 7 DIV under SW treatment. Representative phase contrast images taken on an inverted microscope of AHPC-NSs at 7 DIV post-SW treatment at the following strengths: (A) control treatment, (B) mild treatment, and (C) moderate treatment. Scale bar = 100 μm. Representative fluorescence images of AHPC-NSs at (D) 3 DIV and (E) 7 DIV, following various SW treatment strengths: nonexposed control, mild treatment, and moderate treatment. Cells were stained with PI, a marker to indicate dead cells (PI, red) and cell nuclei marker (DAPI, blue). Cells intentionally killed with 70% ethanol acted as a positive reagent control for PI staining. Scale bar = 100 μm. (F) Quantitative analysis of AHPC-NS viability after 3 and 7 DIV at mild and moderate SW treatment strengths. At both the 3 and 7 DIV time points, there was a significant difference between all three conditions with increased SW strength resulting in increased percentage of PI^+ cells. Bars represent the mean percentage of PI-labeled cells, and the error bars represent the standard error of the mean. N = 3 independent experiments, 18 image fields were quantified for each condition.

in that the dead cells appeared to be spread throughout the NSs rather than being concentrated within a certain area.

Quantitative analysis showed a near stepwise significant increase in the percentage of PI-labeled cells with increasing SW treatment strength at both 3 and 7 DIV post-treatment (Figure 5F). The moderate treatment resulted in the highest percentage of cell death with 12.5−14% of cells being positively labeled with the PI stain (Figure 5F). There was not a significant difference between the conditions over time. Given the percentage of PI-labeled cells within the SW-exposed conditions did not appreciably change from the 3 DIV time point to the 7 DIV time point, this indicated that there was no recovery of the cell health over time. Overall, these results highlighted the negative impact of the SW pulses on the viability of the cells within the NSs, supporting our hypothesis that this SW treatment paradigm could potentially be used to develop a model for TBI. Further modeling is needed to determine what these SW strengths are comparable to in vivo (e.g., falling and hitting your head, impact resulting from a car accident, etc.).

3.2.2. Proliferation Analysis. In addition to a decrease in cell viability within the AHPC-NSs following SW treatment, there also appeared to be a decrease in proliferation and differentiation following treatment. Representative fluorescence images are shown in Figure 6A−I. Regarding cell proliferation, the level of Ki67-immunolabeling appeared to decrease from the control, to the mild, to the moderate SW treatment, though the changes did not appear as striking as those seen for the cell viability results (Figure 5). The quantitative results indicated there were no significant differences in Ki67 expression between any of the conditions, though there was a trend of decreasing proliferation with increased SW strength with the moderate strength having the lowest level of Ki67 expression at 3.5% compared to the 4.7% expression seen for the control condition (Figure 6J). These results again support the hypothesis that SW treatment negatively impacts the health of the AHPC-NSs by negatively influencing proliferation within the NSs.

3.2.3. Differentiation Analysis. In terms of neuronal differentiation, there was also a trend of decreased expression of neuronal-specific cell markers with increased SW strength. The results of the immunocytochemical analysis showed that the control samples had the highest level of TuJ1 and MAP2ab staining, indicative of greater neuronal differentiation (Figure 6A−I). Moderate SW treatment resulted in the lowest percentage of both TuJ1 and MAP2ab-immunolabeling with

https://doi.org/10.1021/acsami.4c08026
ACS Appl. Mater. Interfaces XXXX, XXX, XXX−XXX

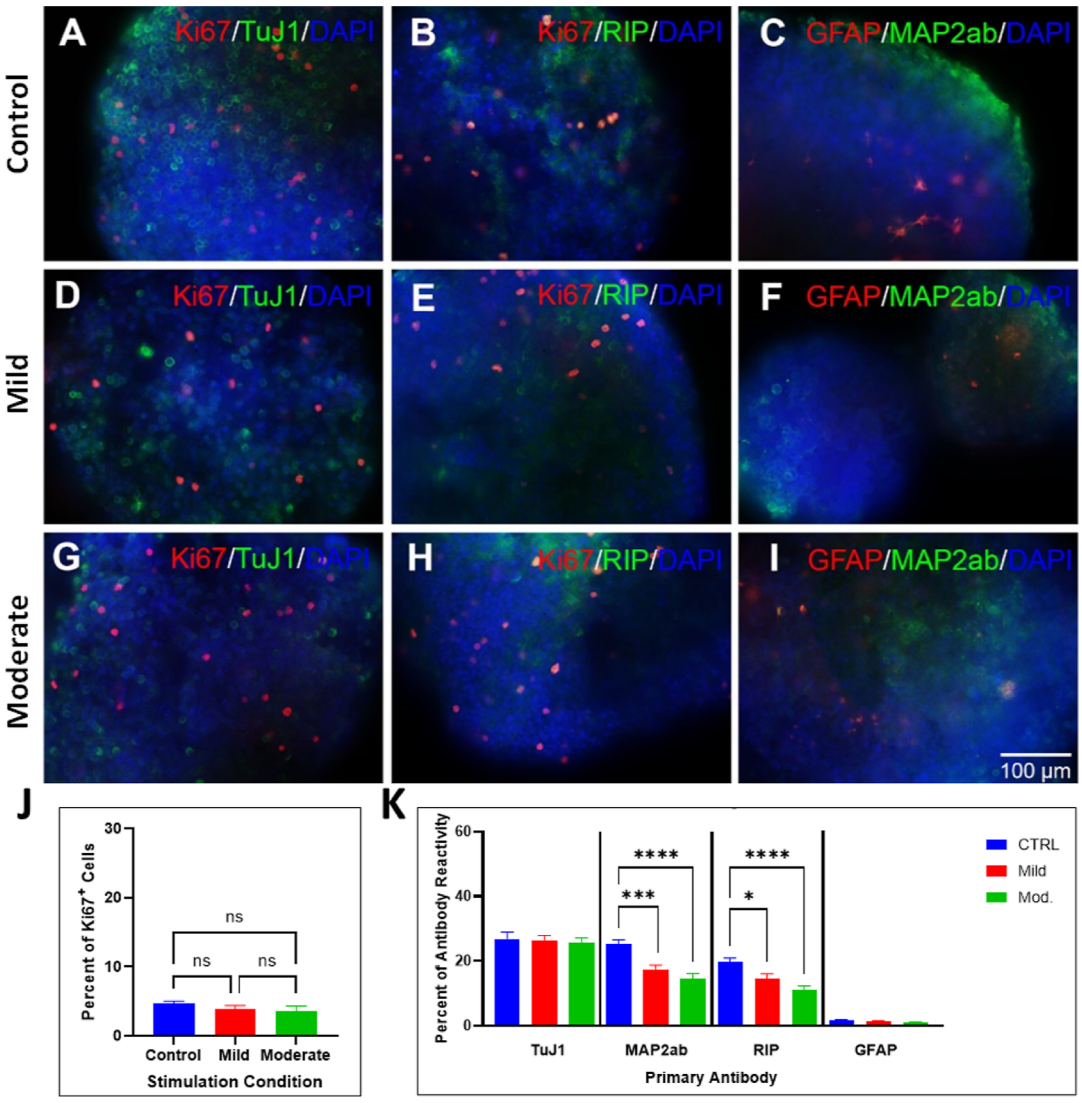

Figure 6. Differentiation of AHPC-NSs at 7 DIV under SW treatment. Fluorescence images of AHPC-NSs at 7 DIV following various SW treatment strengths. Row 1: the nonexposed control; Row 2: the mild treatment; and Row 3: the moderate treatment. Cells were immunolabeled with cell proliferation marker (Ki67, red; A, B, D, E, G, and H), an immature neuronal marker (TuJ1, green; A, D, and G), a marker of maturing neurons (MAP2ab, green; C, F, and I), an oligodendrocyte marker (RIP, green; B, E, and H), an astrocyte marker (GFAP, red; C, F, and I), and a cell nuclei marker (DAPI, blue; A–I). Scale bar = 100 μm. (J) Quantitative analysis of AHPC-NS cell proliferation at 7 DIV following various SW treatments. No significant difference in expression was seen between any conditions. Bars represent the mean percentage of antibody-labeled cells, and the error bars represent the standard error of the mean. N = 3 independent experiments, 18 image fields were quantified for each condition. (K) Quantitative analysis of AHPC-NS cell differentiation at 7 DIV following various SW treatments. There was a significant decrease in the expression of MAP2ab following mild and moderate SW treatments compared to the control condition. RIP expression also significantly decreased for both the mild and moderate groups compared to the control. No significant difference in TuJ1 or GFAP expression was seen between any conditions. Bars represent the mean percentage of antibody-labeled cells, and the error bars represent the standard error of the mean. N = 3 independent experiments, 18 image fields were quantified for each condition.

the mild SW treatment falling between that and the control (Figure 6A–I). Despite quantitative analysis confirming moderate treatment, they resulted in the lowest percentage of TuJ1 expression, and no significant differences between the conditions were seen (Figure 6K). However, there was a significant decrease in the percentage of MAP2ab-labeled cells following both mild and moderate treatments compared to the control with the percentage dropping from 25.3% for the control to 17.5 or 14.7% for the mild and moderate treatment conditions, respectively (Figure 6K). These results show that while the SW treatment does not have a significant effect on the differentiation of the AHPCs into immature neurons, the SW treatments inhibited the differentiation of these cells into more mature neurons.

A similar trend was observed for glial differentiation. The glial cell antibody markers RIP and GFAP were used to distinguish oligodendrocytes and astrocytes, respectively. RIP expression followed a similar trend to MAP2ab with decreasing expression with increased SW strength. SW treatment showed a significant decrease in RIP expression for both mild and moderate SW treatment conditions compared to the control with the percent of RIP-labeled cells decreasing from 19.7% for the control to 14.6 or 11.2% for the mild and moderate treatment conditions, respectively (Figure 6K). Lastly, astrocyte differentiation seemed to be affected to a lesser

https://doi.org/10.1021/acsami.4c08026
ACS Appl. Mater. Interfaces XXXX, XXX, XXX−XXX

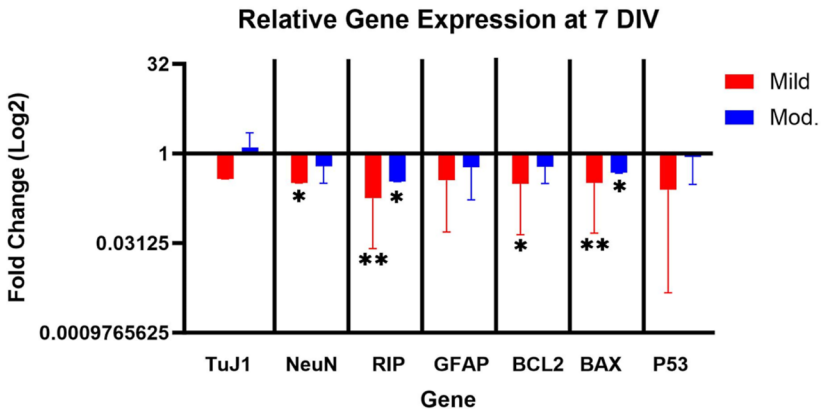

Figure 7. qPCR gene expression analysis of AHPC NSs 7 DIV post-shockwave treatment. qPCR analysis of AHPC-NS cell differentiation at 7 DIV post-SW treatment. Following moderate shockwave treatment, there was a slight increase in TuJ1 gene expression. However, all other genes showed a decrease in expression compared to the control group for both treatment conditions, with the highest amount of repressed expression seen for the mild treatment group. NeuN and BCL2 have significantly lower expression levels compared to the control group following mild shockwave treatment. RIP and BAX showed significantly lower expression levels following both mild and moderate shockwave treatments. Bars represent the Log2 fold change in gene expression of the shockwave-treated groups compared to the nonstimulated control group. The bars above the value of 1 indicate an increase in gene expression while values below the value of 1 indicate decreases in gene expression. $N = 3$ independent experiments.

extent with less apparent changes in GFAP staining seen following SW treatment (Figure 6K). There was no significant difference in GFAP expression between the SW-exposed groups, though there was a slight stepwise decrease in expression with increased SW strength like that seen for the other antibodies evaluated (Figure 6K). The nonsignificant changes in the percentage of GFAP expression could in part be a result of the overall low expression of GFAP present in all conditions. Overall, these differentiation results add further support that the SW treatment negatively impacts the differentiation capabilities of the AHPC-NSs. Despite no significant differences in expression seen for TuJ1 and GFAP following SW treatment compared to nonexposed controls, the expression of these markers decreased with increased SW treatment strength. The significant decreases in expression seen for MAP2ab and RIP labeling following SW treatment showed that SW treatment inhibits (or delays) the differentiation of the AHPCs into more mature neurons as well as inhibits oligodendrocyte differentiation.

3.3. SW Effects on AHPC-NSs: qPCR Gene Expression Analysis. Following the completion of the cell viability and immunocytochemical analyses, which showed an increase in cell death as well as a decrease in the protein expression of many of the markers related to neuronal and glial differentiation, a qRT-PCR analysis was performed to determine if there were any differences in the relative gene expression of several markers related to cell health and differentiation. The qRT-PCR gene expression analysis was consistent with most of the ICC results. At 7 DIV post-treatment, there was a decrease in gene expression for all genes tested following mild SW treatment compared to the control (Figure 7). These negative fold changes corresponded to the decreases observed in the protein expression found for the quantitative analysis of the ICC results for the 7 DIV time point. We found that NeuN had significantly lower expression levels compared to the control group following mild SW treatment (Figure 7). Meanwhile, RIP expression levels showed significantly lower expression levels following both mild and moderate SW treatment (Figure 7). These decreases in gene expression of NeuN and RIP correspond to the decrease in protein expression seen for MAP2ab and RIP, respectively (Figure 6) All genes for both SW treatment conditions showed decreased expression, except TuJ1, following moderate treatment. Despite the increase in relative gene expression for TuJ1 seen following qPCR analysis, there was a decrease in TuJ1 expression following moderate SW treatment seen following ICC analysis. This discrepancy between the gene and protein levels seen for TuJ1 following moderate SW treatment could be the result of translational regulation. Overall, the qPCR analysis corresponds well with the immunocytochemistry results with the SW-exposed conditions showing corresponding decreases in neural gene and protein expression.

Surprisingly, there was a negative fold change in the expression of both pro- and antiapoptotic markers following both mild and moderate SW treatments. The BCL2 gene is a known antiapoptotic gene and its significantly decreased expression following mild SW treatment and slight decrease following moderate SW treatment suggests that there may be an increase in apoptosis following SW treatment, which is supported by the cell viability assay results (Figure 5). However, we also found that BAX and p53, known pro-apoptotic genes, also had decreased expression following both mild and moderate SW treatments, with BAX expression significantly decreased compared to the control for both SW-exposed conditions (Figure 7). It was difficult to interpret these conflicting results for these apoptosis-related genes as we would have expected that a decrease in BCL2 would have a corresponding increase in BAX or p53, or vice versa, which was not found. These conflicting results for the PI cell viability assay and the apoptosis gene expression analysis could be indicative that the increase in cell death seen following SW treatment was due to the cells undergoing necrotic cell death as opposed to programmed cell death.[57]

3.4. SW Effects on AHPC-NSs: Monitoring of Released LDH. Using the fabricated chip shown in Figure 1D, the measurements of LDH released from AHPC-NSs subjected to SW treatment were taken under different time points. The sequence of unplugging the PDMS blockers and allowing the diffusion of the culture media into the eight sensor chambers in sequence is displayed in Figure S6 in Supporting Information.

https://doi.org/10.1021/acsami.4c08026
ACS Appl. Mater. Interfaces XXXX, XXX, XXX−XXX

As shown, the LDH level is quite low on Day 0 (Figure 8). For the single-treatment samples (Treated_1 in Figure 8), the

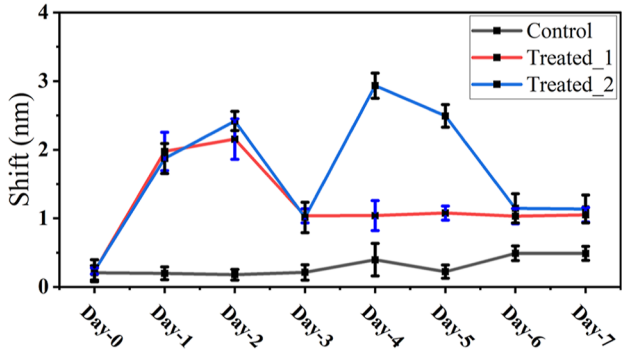

Figure 8. LDH released from AHPC-NSs. Measured transducing signals of LDH released from AHPC-NSs with SW impacts by the sensors at different time points. Control: no SW impact; Treated_1: one SW impact on Day 0; Treated_2: one SW impact on Day 0, followed by the second SW impact on Day 3. $N = 3$ independent experiments.

LDH level increased significantly after the first application 24 h later (on Day 1) and peaked 48 h later (on Day 2). Thereafter, its level started to decrease and plateaued 72 h later (on Day 3), where it remained unchanged for the rest of the study period (i.e., until Day 7 for our experiments) without any additional SW applications (Figure 8). In contrast, when an additional SW application was performed on Day 3 (Treated_2 in Figure 8), the released LDH again significantly increased and peaked in 24 h on Day 4. As shown, on average, the peak LDH level was higher after the second SW application than that after a single SW application. The LDH level started to decrease and eventually reached a similar level to that with only one SW application after 48 h on Day 6. Again, thereafter its level remained unchanged during the rest of the study period (i.e., until Day 7 for our experiments). In comparison with the control, before any SW treatment on the AHPC-NSs, the LDH levels were the same. As shown in Figure 8, the LDH level showed a slight increase from Day 0 and Day 7 for the control.

In contrast, after the NSs were subjected to SW treatment once or twice, the LDH levels showed a clear increase, and even after several days following treatment, the LDH levels remained higher than that of the samples without any SW treatment. It is well-known that the LDH released into the media is directly related to the neural damage due to SW application.[58] Our results support those findings since the first peak in LDH release from the AHPC-NSs cultured in the cell-culture chambers after the first SW application was followed by the second peak in LDH release after the second SW application from the shockwave generator. All these observations are consistent with previously reported results by other research teams.[30,36] Based on these experiments, it is clear this chip can be used for assessing the levels of injuries of AHPC-NSs under SW treatment by monitoring LDH levels. In addition, other molecules released by in vitro brain models under different levels of SW injuries can also be monitored by functionalizing the sensor surface with different antibodies or aptamers specific to the released chemicals. Hence this type of chip is suitable for carrying out experiments to study cellular and molecular features of TBI.

4. CONCLUSIONS

A microchip with integrated sensors has been developed to assess the effects of shockwaves on an in vitro brain model. The brain model is AHPC-NSs. First, the viability, proliferation, and differentiation of cells inside AHPC-NSs subject to SW impacts have been studied. It has been found that the viability, proliferation, and differentiation of cells inside AHPC-NSs have been negatively influenced. A qPCR gene expression analysis was carried out to verify the negative effects of SW impacts. A decrease in gene expression for all genes tested following mild SW treatment compared to the control was detected, thus confirming most of the immunocytochemistry (ICC) results. Then, the effect on the LDH released from AHPC-NSs under SW impacts at different time points was monitored by the integrated sensors adjacent to the cell-culture-chamber on chip. As demonstrated, the LDH levels increased upon the SW impacts while its levels dropped and essentially plateaued, which might be due to some levels of recovery of the injured NSs three days after the SW impacts.[59] But the LDH level was still higher than that released from AHPC-NSs without any SW impacts. Collectively, these features pave the way for in vitro studies of the interactions between the SW and brain models using chip-based technologies, leading to the possible establishment of an in vitro TBI model on chip. However, it is still currently challenging to accurately model TBI on a chip because of its complexity and limited understanding of its pathophysiology.[17]

■ ASSOCIATED CONTENT

Supporting Information

The Supporting Information is available free of charge at https://pubs.acs.org/doi/10.1021/acsami.4c08026.

Fabrication process flow and operation of the sensors, simulation model, and validation of shockwave on neurospheres (PDF)

■ AUTHOR INFORMATION

Corresponding Authors

Donald S. Sakaguchi − *Molecular, Cellular, and Developmental Biology Program, Department of Genetics, Development and Cell Biology, Neuroscience Program, and Nanovaccine Institute, Iowa State University, Ames, Iowa 50011, United States;* orcid.org/0000-0003-4537-0972; Email: dssakagu@iastate.edu

Long Que − *Department of Electrical and Computer Engineering, Iowa State University, Ames, Iowa 50011, United States;* orcid.org/0000-0002-1603-4219; Email: lque@iastate.edu

Authors

Md Fazlay Rubby − *Department of Electrical and Computer Engineering, Iowa State University, Ames, Iowa 50011, United States*

Catherine Fonder − *Molecular, Cellular, and Developmental Biology Program, Department of Genetics, Development and Cell Biology, and Nanovaccine Institute, Iowa State University, Ames, Iowa 50011, United States*

Sajid Uchayash − *Department of Electrical and Computer Engineering, Iowa State University, Ames, Iowa 50011, United States*

https://doi.org/10.1021/acsami.4c08026
ACS Appl. Mater. Interfaces XXXX, XXX, XXX−XXX

Xiaogan Liang − *Department of Mechanical Engineering, University of Michigan at Ann Arbor, Ann Arbor, Michigan 48109, United States;* orcid.org/0000-0002-7390-9130

Complete contact information is available at: https://pubs.acs.org/10.1021/acsami.4c08026

Author Contributions

¶M.F.R. and C.F. contributed equally to this paper.

Notes

The authors declare no competing financial interest.

■ ACKNOWLEDGMENTS

This research was funded in part by NSF Award ECCS 2024797 and the Stem Cell Biology Support Fund. The authors would like to thank Subin Mao's help in this project at the initial stage.

■ REFERENCES

(1) Bryant, R. Post-traumatic stress disorder vs traumatic brain injury. *Dialogues Clin. Neurosci.* **2011**, *13* (3), 251−262.
(2) Wiles, M. Management of traumatic brain injury: a narrative review of current evidence. *Anaesthesia* **2022**, *77*, 102−112.
(3) Mikkonen, E.; Raj, R.; Skrifvars, M. Epidemiology, Outcomes, and Costs of Pediatric Traumatic Brain Injury Treated in the ICU. *Annual Update in Intensive Care and Emergency Medicine 2023*; Springer, 2023; pp 453−466.
(4) Humphreys, I.; Wood, R. L.; Phillips, C. J.; Macey, S. The costs of traumatic brain injury: a literature review. *Clinicoecon. Outcomes Res.* **2013**, *2013*, 281−287.
(5) Wu, Y.-H.; Rosset, S.; Lee, T.-r.; Dragunow, M.; Park, T.; Shim, V. In vitro models of traumatic brain injury: A systematic review. *J. Neurotrauma* **2021**, *38* (17), 2336−2372.
(6) Linseman, D.; Koza, L. Glutathione precursors shield the brain from trauma. *Neural Regener. Res.* **2019**, *14* (10), 1701.
(7) Daneshvar, D. H.; Riley, D. O.; Nowinski, C. J.; McKee, A. C.; Stern, R. A.; Cantu, R. C. Long-term consequences: effects on normal development profile after concussion. *Physical Medicine and Rehabilitation Clinics* **2011**, *22* (4), 683−700.
(8) Mayer, A. R.; Quinn, D. K.; Master, C. L. The spectrum of mild traumatic brain injury: a review. *Neurology* **2017**, *89* (6), 623−632.
(9) Kobeissy, F.; Dixon, C. E.; Hayes, R. L.; Mondello, S. *Injury Models of the Central Nervous System*; Springer, 1940; .
(10) Lighthall, J. W. Controlled cortical impact: a new experimental brain injury model. *J. Neurotrauma* **1988**, *5* (1), 1−15.
(11) Dixon, C. E.; Lyeth, B. G.; Povlishock, J. T.; Findling, R. L.; Hamm, R. J.; Marmarou, A.; Young, H. F.; Hayes, R. L. A fluid percussion model of experimental brain injury in the rat. *J. Neurosurg.* **1987**, *67* (1), 110−119.
(12) Marmarou, A.; Foda, M. A. A.-E.; Brink, W. v. d.; Campbell, J.; Kita, H.; Demetriadou, K. A new model of diffuse brain injury in rats: Part I: Pathophysiology and biomechanics. *J. Neurosurg.* **1994**, *80* (2), 291−300.
(13) Leung, L. Y.; VandeVord, P. J.; Dal Cengio, A. L.; Bir, C.; Yang, K. H.; King, A. I. Blast related neurotrauma: a review of cellular injury. *Molecular & cellular biomechanics* **2008**, *5* (3), 155.
(14) Arun, P.; Spadaro, J.; John, J.; Gharavi, R. B.; Bentley, T. B.; Nambiar, M. P. Studies on blast traumatic brain injury using in-vitro model with shock tube. *Neuroreport* **2011**, *22* (8), 379−384.
(15) Morrison, B., III; Elkin, B. S.; Dollé, J. P.; Yarmush, M. L. In vitro models of traumatic brain injury. *Annu. Rev. Biomed. Eng.* **2011**, *13*, 91−126.
(16) Risdall, J. E.; Menon, D. K. Traumatic brain injury. *Philos. Trans. R. Soc., B* **2011**, *366* (1562), 241−250.
(17) Zhao, Q.; Zhang, J.; Li, H.; Li, H.; Xie, F. Models of traumatic brain injury-highlights and drawbacks. *Front. Neurol.* **2023**, *14*, 1151660.
(18) Shuler, M. L.; Hickman, J. J. Toward in vitro models of brain structure and function. *Proc. Natl. Acad. Sci. U.S.A.* **2014**, *111* (38), 13682−13683.
(19) Surendrakumar, S.; Rabelo, T. K.; Campos, A. C. P.; Mollica, A.; Abrahao, A.; Lipsman, N.; Burke, M. J.; Hamani, C. Neuromodulation therapies in pre-clinical models of traumatic brain injury: systematic review and translational applications. *J. Neurotrauma* **2023**, *40* (5−6), 435−448.
(20) Dams-O'Connor, K.; Juengst, S. B.; Bogner, J.; Chiaravalloti, N. D.; Corrigan, J. D.; Giacino, J. T.; Harrison-Felix, C. L.; Hoffman, J. M.; Ketchum, J. M.; Lequerica, A. H.; et al. Traumatic brain injury as a chronic disease: insights from the United States Traumatic Brain Injury Model Systems Research Program. *Lancet Neurol.* **2023**, *22* (6), 517−528.
(21) Dollé, J. P.; Morrison, B., III; Schloss, R. S.; Yarmush, M. L. Brain-on-a-chip microsystem for investigating traumatic brain injury: Axon diameter and mitochondrial membrane changes play a significant role in axonal response to strain injuries. *Technology* **2014**, *02* (02), 106−117.
(22) Dollé, J. P.; Morrison III, B.; Schloss, R. S.; Yarmush, M. L. An organotypic uniaxial strain model using microfluidics. *Lab Chip* **2013**, *13* (3), 432−442.
(23) Forro, C.; Caron, D.; Angotzi, G. N.; Gallo, V.; Berdondini, L.; Santoro, F.; Palazzolo, G.; Panuccio, G. Electrophysiology read-out tools for brain-on-Chip biotechnology. *Micromachines* **2021**, *12* (2), 124.
(24) Park, T.-E.; Mustafaoglu, N.; Herland, A.; Hasselkus, R.; Mannix, R.; FitzGerald, E. A.; Prantil-Baun, R.; Watters, A.; Henry, O.; Benz, M.; et al. Hypoxia-enhanced Blood-Brain Barrier Chip recapitulates human barrier function and shuttling of drugs and antibodies. *Nat. Commun.* **2019**, *10* (1), 2621.
(25) Bastiaens, A.; Sabahi-Kaviani, R.; Luttge, R. Nanogrooves for 2D and 3D microenvironments of SH-SY5Y cultures in brain-on-chip technology. *Front. Neurosci.* **2020**, *14*, 666.
(26) Nogueira, G. O.; Garcez, P. P.; Bardy, C.; Cunningham, M. O.; Sebollela, A. Modeling the human brain with ex vivo slices and in vitro organoids for translational neuroscience. *Front. Neurosci.* **2022**, *16*, 838594.
(27) Mobini, S.; Song, Y. H.; McCrary, M. W.; Schmidt, C. E. Advances in ex vivo models and lab-on-a-chip devices for neural tissue engineering. *Biomaterials* **2019**, *198*, 146−166.
(28) Alfadil, E.; Bradke, F.; Dupraz, S. In situ visualization of axon growth and growth cone dynamics in acute ex vivo embryonic brain slice cultures. *J. Visualized Exp.* **2021**, *176*, No. e63068.
(29) Rogers, E. A.; Beauclair, T.; Martinez, J.; Mufti, S. J.; Kim, D.; Sun, S.; Stingel, R. L.; Dieterly, A. M.; Krishnan, N.; Crodian, J.; et al. The contribution of initial concussive forces and resulting acrolein surge to β-amyloid accumulation and functional alterations in neuronal networks using a TBI-on-a-chip model. *Lab Chip* **2023**, *23*, 3388−3404.
(30) Shi, W.; Dong, P.; Kuss, M. A.; Gu, L.; Kievit, F.; Kim, H. J.; Duan, B. Design and evaluation of an in vitro mild traumatic brain injury modeling system using 3D printed mini impact device on the 3D cultured human iPSC derived neural progenitor cells. *Adv. Healthcare Mater.* **2021**, *10* (12), 2100180.
(31) Visser, K.; Koggel, M.; Blaauw, J.; van der Horn, H. J.; Jacobs, B.; van der Naalt, J. Blood-based biomarkers of inflammation in mild traumatic brain injury: A systematic review. *Neurosci. Biobehav. Rev.* **2022**, *132*, 154−168.
(32) Mao, S.; Fonder, C.; Rubby, M. F.; Phillips, G. J.; Sakaguchi, D. S.; Que, L. An integrated microfluidic chip for studying the effects of neurotransmitters on neurospheroids. *Lab Chip* **2023**, *23* (6), 1649−1663.
(33) Yang, R.; Fonder, C.; Sylvester, T.; Peng, S.; Jiles, D.; Sakaguchi, D. S.; Que, L. A microfluidic chip for growth and characterization of adult rat hippocampal progenitor cell neurospheroids. *J. Microelectromech. Syst.* **2022**, *31* (1), 37−44.
(34) Yang, R.; Kozik, E.; Patel, B.; Jiles, D.; Sakaguchi, D.; Que, L. In *Studies of Neurospheres Cultured Using Adult Hippocampal Progenitor*

Cells under Off-Chip Magnetic Stimulation; *2019 20th International Conference on Solid-State Sensors, Actuators and Microsystems & Eurosensors XXXIII (TRANSDUCERS & EUROSENSORS XXXIII)*, IEEE: 2019; pp 756−759.
(35) Izumi, Y.; Izumi, M.; Benz, A. M.; Zorumski, C. F. Lactate dehydrogenase release is facilitated by brief sonication of rat hippocampal slices and isolated retinas following acute neuronal damage. *J. Neurosci. Methods* **2001**, *108* (1), 49−55.
(36) Lin, H.; Muramatsu, R.; Maedera, N.; Tsunematsu, H.; Hamaguchi, M.; Koyama, Y.; Kuroda, M.; Ono, K.; Sawada, M.; Yamashita, T. Extracellular lactate dehydrogenase a release from damaged neurons drives central nervous system angiogenesis. *EBioMedicine* **2018**, *27*, 71−85.
(37) Klein, R.; Nagy, O.; Tóthová, C.; Chovanová, F. Clinical and diagnostic significance of lactate dehydrogenase and its isoenzymes in animals. *Vet. Med. Int.* **2020**, *2020*, 5346483.
(38) LaPlaca, M. C.; Lee, V. M.-Y.; Thibault, L. E. An in vitro model of traumatic neuronal injury: loading rate-dependent changes in acute cytosolic calcium and lactate dehydrogenase release. *J. Neurotrauma* **1997**, *14* (6), 355−368.
(39) Snapper, D. M.; Reginauld, B.; Liaudanskaya, V.; Fitzpatrick, V.; Kim, Y.; Georgakoudi, I.; Kaplan, D. L.; Symes, A. J. Development of a novel bioengineered 3D brain-like tissue for studying primary blast-induced traumatic brain injury. *J. Neurosci. Res.* **2023**, *101* (1), 3−19.
(40) Song, C.; Deng, P.; Que, L. Rapid multiplexed detection of beta-amyloid and total-tau as biomarkers for Alzheimer's disease in cerebrospinal fluid. *Nanomed. Nanotechnol. Biol. Med.* **2018**, *14* (6), 1845−1852.
(41) Mao, S.; Fonder, C.; Rubby, F.; Yang, R.; Phillips, G.; Sakaguchi, D.; Que, L. In A Microchip For Studying the Effects of Dopamine and its Precursor On Neurospheroids; *2022 IEEE 35th International Conference on Micro Electro Mechanical Systems Conference (MEMS)*, IEEE: 2022; pp 305−308.
(42) Zhang, T.; Gong, Z.; Giorno, R.; Que, L. A nanostructured Fabry-Perot interferometer. *Opt. Express* **2010**, *18* (19), 20282−20288.
(43) Auersperg, V.; Trieb, K. Extracorporeal shock wave therapy: an update. *EFORT Open Rev.* **2020**, *5* (10), 584−592.
(44) Reznik, J.; Biros, E.; Lamont, A.; Sacher, Y.; Kibrik, O.; Milanese, S.; Gordon, S.; Galea, M. A preliminary investigation on the effect of extracorporeal shock wave therapy as a treatment for neurogenic heterotopic ossification following traumatic brain injury. Part I: effects on pain. *Brain Inj.* **2017**, *31* (4), 526−532.
(45) Attenborough, K.; Postema, M. *A Pocket-Sized Introduction to Acoustics*; Univerisity of Hull, 2008.
(46) Bies, D. A.; Hansen, C. H.; Howard, C. Q. *Engineering Noise Control*; CRC Press, 2017.
(47) Roeser, R. J.; Valente, M.; Hosford-Dunn, H. Diagnostic procedures in audiology. *Audiology: Diagnosis*; Springer, 2007; pp 1−16.
(48) Sound pressure. https://en.wikipedia.org/wiki/Sound_pressure. date of access: June 4, 2024.
(49) Okwara, C. K.; Vaez Ghaemi, R.; Yu, C.; Le, M.; Yadav, V. G.; Frostad, J. M. The mechanical properties of neurospheres. *Adv. Eng. Mater.* **2021**, *23* (8), 2100172.
(50) Yang, R.; Boldrey, J.; Jiles, D.; Schneider, I.; Que, L. On chip detection of glial cell-derived neurotrophic factor secreted from dopaminergic cells under magnetic stimulation. *Biosens. Bioelectron.* **2021**, *182*, 113179.
(51) Zhang, T.; He, Y.; Wei, J.; Que, L. Nanostructured optical microchips for cancer biomarker detection. *Biosens. Bioelectron.* **2012**, *38* (1), 382−388.
(52) Palmer, T. D.; Takahashi, J.; Gage, F. H. The adult rat hippocampus contains primordial neural stem cells. *Mol. Cell. Neurosci.* **1997**, *8* (6), 389−404.
(53) Ye, J.; Coulouris, G.; Zaretskaya, I.; Cutcutache, I.; Rozen, S.; Madden, T. L. Primer-BLAST: a tool to design target-specific primers for polymerase chain reaction. *BMC Bioinf.* **2012**, *13*, 134.
(54) Raymond, J. L.; Haworth, K. J.; Bader, K. B.; Radhakrishnan, K.; Griffin, J. K.; Huang, S.-L.; McPherson, D. D.; Holland, C. K. Broadband attenuation measurements of phospholipid-shelled ultrasound contrast agents. *Ultrasound Med. Biol.* **2014**, *40* (2), 410−421.
(55) Eskandari, F.; Rahmani, Z.; Shafieian, M. The effect of large deformation on Poisson's ratio of brain white matter: An experimental study. *Proc. IME H J. Eng. Med.* **2021**, *235* (4), 401−407.
(56) Milo, R.; Phillips, R. What is the Density of Cells. *Cell Biol.* **2013**, *2015*, 1−5.
(57) Hutchins, J. B.; Barger, S. W. Why neurons die: cell death in the nervous system. *Anat. Rec.* **1998**, *253* (3), 79−90.
(58) Jin, H.; Bi, R.; Hu, J.; Xu, D.; Su, Y.; Huang, M.; Peng, Q.; Li, Z.; Chen, S.; Hu, B. Elevated serum lactate dehydrogenase predicts unfavorable outcomes after rt-PA thrombolysis in ischemic stroke patients. *Front. Neurol.* **2022**, *13*, 816216.
(59) Valvona, C. J.; Fillmore, H. L.; Nunn, P. B.; Pilkington, G. J. The regulation and function of lactate dehydrogenase a: therapeutic potential in brain tumor. *Brain Pathol.* **2016**, *26* (1), 3−17.

https://doi.org/10.1021/acsami.4c08026
ACS Appl. Mater. Interfaces XXXX, XXX, XXX−XXX